

Outage Analysis of Aerial Semi-Grant-Free NOMA Systems

Hongjiang Lei, Chen Zhu, Ki-Hong Park, Imran Shafique Ansari,
Weijia Lei, Hong Tang, and Kyeong Jin Kim

Abstract—In this paper, we analyze the outage performance of Unmanned Aerial Vehicles (UAVs)-enabled downlink Non-Orthogonal Multiple Access (NOMA) communication systems with the Semi-Grant-Free (SGF) transmission scheme. A UAV provides coverage services for a Grant-Based (GB) user and one Grant-Free (GF) user is allowed to utilize the same channel resource opportunistically. The analytical expressions for the exact and asymptotic Outage Probability (OP) of the GF user are derived. The results demonstrate that no-zero diversity order can be achieved only under stringent conditions on users' quality of service requirements. Subsequently, an efficient Dynamic Power Allocation (DPA) scheme is proposed to relax such data rate constraints. The analytical expressions for the exact and asymptotic OP of the GF user with the DPA scheme are derived. Finally, Monte Carlo simulation results are presented to validate the correctness of the derived analytical expressions and demonstrate the effects of the UAV's location and altitude on the OP of the GF user.

Index Terms—Unmanned aerial vehicle, non-orthogonal multiple access, semi-grant-free, outage probability.

I. INTRODUCTION

A. Background and related works

In recent years, Unmanned Aerial Vehicles (UAVs) have been envisioned to play an essential role in space-air-ground integrated networks due to the flexibility of deployment, controllable mobility, and low costs [1]. Multiple access techniques are essential to integrate UAVs into 5G networks and beyond. Non-Orthogonal Multiple Access (NOMA) is regarded as a profitable candidate for 5G networks because of its merit in providing higher Spectral Efficiency (SE) and supporting massive connectivity [2]. Multiple users are served simultaneously in non-orthogonal channel resources by isolating the users in the power domain [3]. Using NOMA

technology, UAVs can provide services for multiple users over the same resource block. Quite a few current investigations have considered using NOMA to improve the performance of UAV-enabled communication systems. Hou *et al.* focused on addressing the spatial distribution problem of NOMA-enhanced UAV network by utilizing stochastic geometry tools [4]–[7]. In [4], a new 3D UAV framework for downlink wireless service to randomly roaming NOMA users was proposed. Analytical expressions for the Outage Probability (OP) and Ergodic Capacity (EC) of Multiple-Input-Multiple-Output (MIMO)-NOMA-enhanced UAV networks were derived. In [5], the NOMA-enhanced UAV-to-everything networks were investigated. The closed-form expressions for the OP and EC of the paired NOMA receivers were derived. In [6], the UAV-centric strategy for offloading actions and the user-centric strategy for providing emergency network were considered, and the analytical expressions of the Coverage Probability (CP) for both scenarios with imperfect Successive Interference Cancellation (SIC) were derived.

NOMA-enhanced terrestrial Internet of Things (IoT) networks and NOMA-enhanced aerial IoT networks were investigated in [7], and new channel statistics were derived for both terrestrial and aerial users. Then, the analytical expressions for the exact and the asymptotic coverage probability were derived. To maximize the sum capacity of NOMA-enabled backscatter communication systems, the transmit power of IoT users at BS and the reflection coefficient of backscatter tag were jointly optimized in [8]. The convex optimization problems were solved by Karush-Kuhn-Tucker conditions.

Performance optimization of NOMA-aided UAV systems has been well-researched in many works. In [9], a UAV-assisted NOMA system was studied where the UAV assisted the Base Station (BS) in providing services to the ground users. The sum rate was maximized by optimizing the UAV trajectory and the NOMA precoding. In [10], an aerial Decode-and-Forward (DF) cooperative NOMA network was jointly optimized concerning UAV height, channel allocation, and power allocation to maximize the data rate. Ref. [11] considered the Energy Efficiency (EE) of the UAV's communication with imperfect channel state information where the EE was maximized by designing user scheduling and power allocation. Authors in [12] proposed a time-efficient data collection scheme where multiple ground devices upload their data to the UAV via uplink NOMA. The duration of each time slot was minimized by jointly optimizing the trajectory, device scheduling, and transmit power. In [13], the location of the UAV and power allocation were jointly optimized to enhance

This work was supported by the National Natural Science Foundation of China under Grant 61971080 and the Open Fund of the Shaanxi Key Laboratory of Information Communication Network and Security under Grant ICNS201807.

Hongjiang Lei, Chen Zhu, Weijia Lei, and Hong Tang are with the School of Communication and Information Engineering, Chongqing University of Posts and Telecommunications, Chongqing 400065, China, also with Chongqing Key Lab of Mobile Communications Technology, Chongqing 400065, China, and H. Lei is also with Shaanxi Key Laboratory of Information Communication Network and Security, Xi'an University of Posts and Telecommunications, Xi'an, Shaanxi 710121, China (e-mail: leihi@cqupt.edu.cn).

Ki-Hong Park is with CEMSE Division, King Abdullah University of Science and Technology (KAUST), Thuwal 23955-6900, Saudi Arabia (e-mail: kihong.park@kaust.edu.sa).

Imran Shafique Ansari is with James Watt School of Engineering, University of Glasgow, Glasgow G12 8QQ, United Kingdom (e-mail: imran.ansari@glasgow.ac.uk).

Kyeong Jin Kim is with the Mitsubishi Electric Research Laboratories, Cambridge, MA 02139 USA (e-mail: kkim@merl.com).

the EE and SE of NOMA-aided UAV systems.

Conventional wireless communication systems operate on Grant-Based (GB) protocols [14]. Each device first transmits a scheduling request to BS and then sends a grant back for resource allocation. The lengthy handshaking process of requesting a grant will be prohibitively costly for the signaling overhead and unacceptable for the resulting latency in massive IoT data transmissions [15]. Ding *et al.* proposed NOMA-assisted Semi-Grant-Free (SGF) transmission schemes and two contention control mechanisms have been presented to ensure that the number of users admitted to the same channel was carefully controlled in [16]. And then, a new SGF transmission scheme combining the flexibility in choosing the decoding order in NOMA was proposed. The closed-form expressions for the exact and asymptotic OP were derived. The results show that the NOMA-assisted SGF transmission scheme effectively addresses the problem of the aforementioned request-grant process and the spectrum reserved. Based on [16], a new Power Control (PC) strategy was proposed to guarantee no OP floor entirely by adjusting the transmit power of Grant-Free (GF) user to control the decoding order of SIC at the base station in [17]. In [18], an adaptive power allocation strategy was proposed founded on the relationship between the target data rate of GB users and channel conditions of both GB and GF users. Authors in [19] considered a NOMA system with multiple randomly distributed GF users. The analytical expressions for the OP with fixed transmit power and dynamic power control strategy were derived, and the small-scale fading, path loss, and random user locations were considered. Furthermore, the outage performance of GF users was analyzed under the best user scheduling scheme and Cumulative Distribution Function (CDF)-based scheduling scheme. In [20], an uplink SGF NOMA system with multiple randomly deployed GF users was studied by utilizing stochastic geometry techniques. A dynamic protocol was proposed to interpret part of the GF users that are paired to NOMA groups. The outage performance and diversity gains under dynamic and open-loop protocols were investigated, and numerical results show that dynamic protocol effectively improves the outage performance. Moreover, the analytical expressions for the exact and approximated EC were derived in [21]. The secrecy performance of NOMA-aided SGF was investigated in [22] wherein the analytical expressions for the Secrecy Outage Probability (SOP) for the scenarios with a single GF user and multiple GF users were derived, respectively. In [23], an Intelligent Reconfigurable Surface (IRS)-assisted SGF NOMA system was investigated, in which the IRS enhanced the channel gains for GB and GF users. The sum rates of GF users were maximized by jointly optimizing the sub-carrier assignment, the power allocation of GF users, and the IRS amplitude and phase shift.

Table I outlines related works on performance analysis of NOMA-aided SGF systems.

B. Motivation and contributions

In light of the above-discussed works, the performance of uplink NOMA systems with the SGF scheme has been studied

in varying scenarios. However, there still needs to be more research contributions on investigating the performance of UAV communication systems with the SGF scheme, which motivates this work. In this work, we dedicate ourselves to developing new SGF schemes utilized in UAV-enabled downlink NOMA communication systems. The impacts of the UAV's location and altitude on outage performance are studied. The main contributions of this paper are outlined as follows:

- 1) We investigate the outage performance of the GF user and the analytical expression for the exact OP is derived. We also analyze the asymptotic OP and the achievable diversity orders in the higher-signal-to-noise ratio (SNR) region to obtain more insights. The results demonstrate that no-zero diversity order can be achieved only under stringent conditions on users' quality of service requirements.
- 2) An efficient Dynamic Power Allocation (DPA) scheme is proposed to guarantee no floor without any conditions on users' target rates. The analytical expressions for the exact and asymptotic OP of the GF user with the DPA scheme are derived. The results demonstrate no OP floor for all the users' target rates when the DPA scheme is utilized.
- 3) Monte Carlo simulation results are presented to validate the correctness of the derived analytical expressions and demonstrate the effects of the UAV's location and altitude on the OP of the GF user.
- 4) Relative to [16] - [19] wherein the performance of the uplink NOMA-aided SGF systems was investigated, the transmit power and the Channel State Information (CSI) of GB users must be known at the GF user to realize the power control. This work studied the performance of the downlink NOMA-aided SGF systems, where the power allocation is utilized at the base station and the GF user need not know the CSI of the GB user.

C. Organization

The rest of this paper is organized as follows. Section II describes the considered system model and the SGF scheme utilizing in downlink NOMA systems. The OP of the GF user with Fixed Power Allocation (FPA) and DPA are analyzed in Sections III and IV, respectively. Section V presents the simulation results to demonstrate the analysis and the paper is concluded in Section VI.

II. SYSTEM MODEL

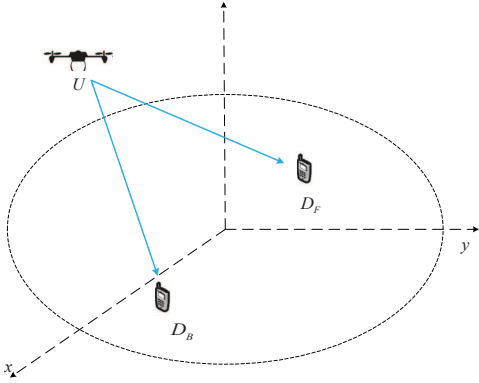
A. System model

As shown in Fig. 1, we consider a UAV-enabled downlink NOMA system that consists of an aerial base station (U), a GB user (D_B), and a GF user (D_F)¹. Similar to [16], D_B is allocated to one dedicated resource block and D_F will gain admission to the resource block opportunistically. Without loss

¹Although only two users are considered in this work, our results can be easily extended to NOMA systems with more than two users by utilizing the hybrid multiple access scheme proposed in [24], [25], [26].

TABLE I: Recent literature related to performance analysis of NOMA-aided SGF systems.

Reference	downlink/uplink NOMA	UAV	Method	Performance Metrics
[4]	downlink	✓	Performance analysis	OP, EC
[5]	downlink	✓	Performance analysis	OP, EC
[6]	downlink	✓	Performance analysis	CP
[7]	uplink	✓	Performance analysis	CP
[8]	downlink		Optimization	Sum rate
[9]	downlink	✓	Optimization	Sum rate
[10]	downlink	✓	Optimization	Sum rate
[11]	downlink	✓	Optimization	EE
[12]	uplink	✓	Optimization	Flight time
[13]	uplink	✓	Optimization	SE, EE
[16]	uplink, SGF		Performance analysis	OP
[17]	uplink, SGF		Performance analysis	OP
[18]	uplink, SGF		Performance analysis	OP
[19]	uplink, SGF		Performance analysis	OP
[20]	uplink, SGF		Performance analysis	OP
[21]	uplink, SGF		Performance analysis	EC
[22]	uplink, SGF		Performance analysis	SOP
[23]	uplink, SGF		Deep reinforcement learning	Average data rate

Fig. 1: A downlink UAV-based NOMA communication system consisting of one UAV (U) and two legitimate users (D_B and D_F).

of generality, a 3D cartesian coordinate system with the origin at O is utilized. The coordinates of D_B and D_F are denoted as $(x_B, y_B, 0)$ and $(x_F, y_F, 0)$, respectively. The coordinate of U is denoted as (x_U, y_U, z_U) and the distance between U and D_X ($X \in \{B, F\}$) is expressed as

$$d_X = \sqrt{(x_X - x_U)^2 + (y_X - y_U)^2 + z_U^2} \quad (1)$$

Due to possible obstacles between the Air-to-Ground (A2G) links, Line-of-Sight (LoS) and Non-Line-of-Sight (NLoS) connections are probabilistically considered in this work. As a result, the average path loss between U and D_X is expressed as [27]

$$\bar{g}_X = (P_X^L \eta_L + P_X^{nL} \eta_{nL}) d_X^{\alpha_X} \quad (2)$$

where η_L and η_{nL} signify the attenuation factor to the LoS and NLoS links, respectively, P_X^L signifies the probability of LoS connection, $P_X^L = \left(1 + a_0 e^{-b_0 \left(\frac{180}{\pi} \theta_X - a_0\right)}\right)^{-1}$, a_0 and b_0 are environmental parameters as listed in Table I and II of [28], $\theta_X = \arcsin\left(\frac{H}{d_X}\right)$ denotes elevation angle (in radians),

$P_X^{nL} = 1 - P_X^L$, and α_X is the path loss exponent. The relationship between α_X and θ_X is expressed as [29]

$$\alpha_X(\theta_X) = b_1 P_X^L + b_2 \quad (3)$$

where $b_1 \approx \alpha_{\frac{\pi}{2}} - \alpha_0$ and $b_2 \approx \alpha_0$. In this work, we set $\alpha_{\frac{\pi}{2}} = 2$ and $\alpha_0 = 4$.

It is assumed that the fading coefficients, h_X , in the A2G links experience independent and identically (i.i.d) Nakagami- m fading. Denoting $G_X = \frac{h_X}{\bar{g}_X}$, the Probability Density Function (PDF) and the CDF of G_X are expressed by

$$F_{G_X}(x) = 1 - e^{-\lambda_X x} \sum_{i=0}^{m-1} \frac{(\lambda_X x)^i}{i!} \quad (4)$$

$$f_{G_X}(x) = \frac{\lambda_X^m}{\Gamma(m)} x^{m-1} e^{-\lambda_X x} \quad (5)$$

where m denotes the fading parameter that is integer, $\lambda_X = m\bar{g}_X$, and $\Gamma(\cdot)$ is the Gamma function as defined by [30, (8.310.1)].

B. SGF schemes

To ensure the D_B 's Quality-of-Service (QoS) in the worse scenario, the D_B 's rate is constrained as [16]

$$\log_2 \left(1 + \frac{\rho \omega G_B}{1 + \rho \bar{\omega} G_B} \right) \geq R_{th}^B \quad (6)$$

where $\rho = \frac{P}{\sigma^2}$, P is the transmit power of U , σ^2 is the variance of complex zero mean Additive White Gaussian Noise (AWGN), $0 \leq \omega \leq 1$ denotes the power allocation coefficient for D_B , $\bar{\omega} = 1 - \omega$, and R_{th}^B denotes the Reliability Rate Threshold (RRT) of D_B . Then, we have

$$\omega \geq \frac{(\rho G_B + 1)(\Theta_B - 1)}{\rho G_B \Theta_B} \quad (7)$$

$$\rho \geq \frac{\Theta_B - 1}{G_B (\Theta_B \bar{\omega} - (\Theta_B - 1))} \quad (8)$$

$$G_B \geq \frac{\Theta_B - 1}{\rho(1 - \Theta_B \bar{\omega})} \quad (9)$$

where $\Theta_B = 2^{R_{th}^B}$. Eqs. (7), (8), and (9) denote the conditions in which the power allocation coefficient, the transmission SNR, and the channel coefficient of D_B must meet for the other given parameters.

Remark 1. When $\omega = 1$, one can easily find that decoding its own signal would fail at D_B if $\log_2(1 + \rho G_B) < R_{th}^B$, which means to ensure that D_B decodes its own signal successfully, there is a constraint

$$G_B > \varepsilon_1 \quad (10)$$

where $\varepsilon_1 = \frac{\Theta_B - 1}{\rho}$.

It must be noted that the SGF scheme only guarantees that admitting the GF user is transparent to the GB user whose QoS experience is the same when it occupies the channel alone [22]. In other words, the SGF scheme does not always guarantee no outage for D_B . When the fading over the link between U and D_B is too strong, the constraint in (10) can not be satisfied thereby the SGF scheme can not be utilized because there are no signals to D_F to avoid any performance degradation for D_B .

Considering the decoding order at D_F for given ω and ρ , according to the principle of SIC in NOMA, if the D_B 's signal can be successfully decoded in the first stage of SIC and deleted from the superimposed signal received at D_F , the interference can be eliminated and the maximum achievable rate can be obtained. Because $\log_2\left(1 + \frac{\rho\omega x}{1+\rho\omega x}\right) = \log_2\left(1 + \frac{\rho\omega}{\frac{1}{x}+\rho\omega}\right)$ is an increasing function of x and $\log_2\left(1 + \frac{\rho\omega G_F}{1+\rho\omega G_F}\right) > R_{th}^B$ holds when $G_F > G_B$. Then, the condition of D_F decoding D_B 's signal at the first stage of SIC is $G_F > G_B$. According to this, there are two different decoding orders at D_F , which is stated as follows:

- Case 1: U is located in the region where the channel condition of D_F is stronger than that of D_B , namely $G_F > G_B$. In this scenario, D_B 's signal can be decoded at the first stage or the second stage of SIC. Accordingly, D_F will achieve a data rate of $\log_2(1 + \bar{\omega}\rho G_F)$ or $\log\left(1 + \frac{\bar{\omega}\rho G_F}{1+\rho\omega G_F}\right)$. To maximize its data rate, D_F will decode D_B 's signal at the first stage of SIC due to $\log\left(1 + \frac{\bar{\omega}\rho G_F}{1+\rho\omega G_F}\right) < \log_2(1 + \bar{\omega}\rho G_F)$. Then, the achievable rate of D_F in this scenario is expressed as

$$R_F^1 = \log_2(1 + \bar{\omega}\rho G_F) \quad (11)$$

- Case 2: U is located in the region where the channel condition of D_F is weaker than that of D_B , namely $G_F < G_B$. In this scenario, D_F cannot decode D_B 's signal at the first stage of SIC since $G_F < G_B$ leads to $\log_2\left(1 + \frac{\rho\omega G_F}{1+\rho\omega G_F}\right) < R_{th}^B$. Therefore, D_F must decode its own signal firstly, which achieves the data rate as

$$R_F^2 = \log_2\left(1 + \frac{\bar{\omega}\rho G_F}{1 + \rho\omega G_F}\right) \quad (12)$$

Then, the achievable rate of D_F is expressed as

$$R_F = \begin{cases} R_F^1, & G_F > G_B \\ R_F^2, & G_F < G_B \end{cases} \quad (13)$$

III. OUTAGE PERFORMANCE ANALYSIS WITH FIXED POWER ALLOCATION

Note that when the SGF scheme is adopted, the QoS requirements of the GB user will be met first. The GF user can utilize GB's channel only when the GB user can achieve its target rate. If the outage happens to the GB user, it means that the channel resource is insufficient to meet the QoS requirements of the GB user; therefore, the GF user is not allowed to access the channel, and the GB user occupies the channel alone. Thus, D_B can consistently achieve the same outage performance as in Orthogonal Multiple Access (OMA) and so we only investigate D_F 's outage performance.

In this section, it is assumed that D_B is allocated to a fixed power $\omega = \min\left\{\frac{(\rho G_B + 1)(\Theta_B - 1)}{\rho G_B \Theta_B}, 1\right\}$ that gives priority to meet its QoS requirement. To distinguish the scheme proposed in Section IV, this scheme is termed as FPA scheme. The OP of D_F with the SGF scheme is expressed by

$$P_{out} = \underbrace{\Pr\{G_B < \varepsilon_1\}}_{\triangleq T_0} + \underbrace{\Pr\{G_B > \varepsilon_1, R_F < R_{th}^F\}}_{\triangleq T_1} \quad (14)$$

where R_{th}^F signifies the RRT of D_F , T_0 denotes D_B is in outage when it occupies the channel alone, which means D_F is not allowed to utilize the channel, and T_1 denotes D_F is in outage when it is allowed to utilize D_B 's channel.

Remark 2. When $\rho \rightarrow \infty$, there is $\varepsilon_1 \rightarrow 0$, then $T_0 \rightarrow 0$. Thus, T_0 is the main part of P_{out} in the lower- ρ region while T_1 is the main part of P_{out} in larger- ρ region.

The following theorem provides the analytical expression for the OP of D_F .

Theorem 1. The analytical expression for the OP of D_F is expressed as

$$P_{out}^{FPA} = \begin{cases} T_0 + T_{11} + T_{12a}, & \Theta_{th} < \frac{\Theta_B}{\Theta_B - 1} \\ T_0 + T_{11} + T_{12b}, & \Theta_{th} > \frac{\Theta_B}{\Theta_B - 1} \end{cases} \quad (15)$$

where $\Theta_{th} = 2^{R_{th}^F}$, $T_0 = F_{G_B}(\varepsilon_1)$, $T_{11} = \chi_1 - \chi_2$, $T_{12a} = \chi_3 + \chi_4$, $T_{12b} = \bar{F}_{G_B}(\varepsilon_1) - A_1 \sum_{i=0}^{m-1} \frac{\lambda_F^i \Gamma(i+m, A_2 \varepsilon_1)}{i! A_2^{i+m}}$, $\chi_1 = F_{G_B}(\varepsilon_0) - F_{G_B}(\varepsilon_1) - A_1 \Phi_1$, $\chi_2 = F_{G_B}(\varepsilon_0) - F_{G_B}(\varepsilon_1) - A_1 \sum_{i=0}^{m-1} \frac{\lambda_F^i \Phi_2}{i!}$, $\chi_3 = F_{G_B}(\varepsilon_5) - F_{G_B}(\varepsilon_1) - A_1 \sum_{i=0}^{m-1} \frac{\lambda_F^i \Phi_3}{i!}$, $\chi_4 = \bar{F}_{G_B}(\varepsilon_5) - A_1 \Phi_4$, $\Phi_1 = g_1(\varepsilon_1, \varepsilon_2, \varepsilon_1, \varepsilon_0)$, $\Phi_2 = \frac{\Upsilon(i+m, A_2 \varepsilon_0)}{A_2^{i+m}} - \frac{\Upsilon(i+m, A_2 \varepsilon_1)}{A_2^{i+m}}$, $\Phi_3 = \frac{1}{A_2^{i+m}} (\Upsilon(i+m, A_2 \varepsilon_5) - \Upsilon(i+m, A_2 \varepsilon_1))$, $\Upsilon(\cdot, \cdot)$ is lower incomplete Gamma function as defined by [30, (8.350.2)], $\Phi_4 = g_2(\varepsilon_3, \varepsilon_4, \varepsilon_5)$, $g_1(a, b, s, t) = \frac{\pi}{N} \sum_{i=0}^{m-1} \frac{(\lambda_F b)^i}{i!} \sum_{n=1}^N \frac{(\mu_n(s, t))^{m+i-1}}{(\mu_n(s, t) - a)^i} \sqrt{(\mu_n(s, t) - s)(t - \mu_n(s, t))} e^{-\lambda_B \mu_n(s, t) - \lambda_F b \frac{\mu_n(s, t)}{\mu_n(s, t) - a}}$, $\varepsilon_2 = \frac{\Theta_B(\Theta_{th} - 1)}{\rho}$, $\varepsilon_0 = \varepsilon_1 + \varepsilon_2$, $g_2(a, b, c) = \sum_{i=0}^{m-1} \frac{(\lambda_F b)^i}{i!} \sum_{n=1}^N \left(\frac{\omega_n \mu_n^{m+i-1}}{(\mu_n - a)^i} e^{\mu_n} - \left(\lambda_B \mu_n + \frac{\lambda_F b \mu_n}{\mu_n - a} \right) \right) - \frac{\pi e^{-\left(\lambda_B \mu_n(0, c) + \frac{\lambda_F b \mu_n(0, c)}{\mu_n(0, c) - a} \right)} (\mu_n(0, c))^{m+i-1} \sqrt{\mu_n(0, c)(c - \mu_n(0, c))}}{N(\mu_n(0, c) - a)^i}$.

$$\begin{aligned}
P_{\text{out}}^{\text{DPA}} &= \underbrace{\Pr\{G_B < \varepsilon_1\}}_{\triangleq T_0} + \underbrace{\Pr\{G_B > \varepsilon_1, G_F > G_B, R_F^1 < R_{\text{th}}^F\}}_{\triangleq T_{11}} \\
&+ \underbrace{\Pr\left\{G_B > \varepsilon_1, G_F < \frac{\Theta_B G_B}{\rho G_B + 1}, R_F^2 < R_{\text{th}}^F\right\}}_{\triangleq T_2} + \underbrace{\Pr\left\{G_B > \varepsilon_1, \frac{\Theta_B G_B}{\rho G_B + 1} < G_F < G_B, R_F^3 < R_{\text{th}}^F\right\}}_{\triangleq T_3}
\end{aligned} \quad (19)$$

$$P_{\text{out}}^{\text{DPA}, \infty} = \begin{cases} T_0^\infty + T_{11}^\infty + T_3^\infty, & \Theta_{th} < \frac{\Theta_B}{\Theta_B - 1} \\ T_0^\infty + T_{11}^\infty + T_{2b}^\infty + T_3^\infty, & \Theta_{th} > \frac{\Theta_B}{\Theta_B - 1} \end{cases} \quad (21)$$

$\varepsilon_3 = \frac{\Theta_B - 1}{\rho} \frac{\Theta_{th}}{\Theta_{th} - (\Theta_{th} - 1)\Theta_B}$, $\varepsilon_4 = \frac{\Theta_B(\Theta_{th} - 1)}{(\Theta_B - \Theta_{th}(\Theta_B - 1))\rho}$,
 $\varepsilon_5 = \frac{2\Theta_B\Theta_{th} - \Theta_{th} - \Theta_B}{\rho(\Theta_{th} + \Theta_B - \Theta_{th}\Theta_B)}$, $\bar{F}_{G_X}(x) = 1 - F_{G_X}(x)$,
 $A_1 = \frac{\lambda_B}{\Gamma(m)}$, $A_2 = \lambda_B + \lambda_F$, $\mu_n(s, t) = \frac{t+s}{2} + \frac{(t-s)\tau_n}{2}$,
 $\tau_n = \cos \frac{(2n-1)\pi}{2N}$, N is the summation terms, which reflects accuracy vs. complexity, ι_n is the n th zeros of Laguerre polynomials, and w_n is the Gaussian weight, which are given in Table (25.9) of [31].

Proof: Please refer to Appendix A.

Eq. (15) provides an exact relationship between the OP of D_F and all the system parameters. Some interesting insights can be obtained. Firstly, the requirement of D_B directly determines whether the resources can be shared with D_F . A higher RRT denotes a lower probability of resource sharing. Secondly, the location of S is one of the important factors affecting DF performance because that affects the decoding order on D_F . Thus, the OP of D_F can be minimized by jointly optimizing the location of S and other systems parameters, which will be part of future works. Last but not least, the relationship between the RRT for D_B and D_F users under the condition in which the resources can be shared also significantly impacts the OP of the D_F . The analytical expressions presented in Theorem 1 are complicated because many coupled factors affect the outage performance of the GF user, specifically, the decoding order, the RRT of D_B , the RRT of D_F , and the relationship between D_B 's and D_F 's channel condition.

The asymptotic OP is derived in the following corollary to obtain more insights.

Corollary 1. When $\rho \rightarrow \infty$, the asymptotic OP is expressed as

$$P_{\text{out}}^{\text{FPA}, \infty} = \begin{cases} T_0^\infty + T_{11}^\infty + T_{12a}^\infty, & \Theta_{th} < \frac{\Theta_B}{\Theta_B - 1} \\ T_0^\infty + T_{11}^\infty + T_{12b}^\infty, & \Theta_{th} > \frac{\Theta_B}{\Theta_B - 1} \end{cases} \quad (16)$$

$$\begin{aligned}
\text{where } T_0^\infty &= \frac{(\lambda_B \varepsilon_1)^m}{m!}, T_{11}^\infty \approx \frac{\lambda_B^m (\varepsilon_0^m - \varepsilon_1^m)}{m!} \left(\frac{(\lambda_F \varepsilon_2)^m}{m!} - 1 \right) + \\
&\frac{\lambda_B^m}{\Gamma(m)} \sum_{i=0}^{m-1} \frac{\lambda_F^i (\varepsilon_0^{i+m} - \varepsilon_1^{i+m})}{i!(i+m)}, \quad T_{12a}^\infty = \chi_3^\infty + \chi_4^\infty, \\
\chi_3^\infty &\approx \frac{\lambda_B^m (\varepsilon_5^m - \varepsilon_1^m)}{m!} - A_1 \sum_{i=0}^{m-1} \frac{\lambda_F^i (\varepsilon_5^{i+m} - \varepsilon_1^{i+m})}{i!(i+m)}, \\
\chi_4^\infty &\approx \frac{(\lambda_F \varepsilon_4)^m}{m!} \left(1 - \frac{(\lambda_B \varepsilon_5)^m}{m!} \right), \quad \text{and} \quad T_{12b}^\infty \approx \\
1 - \frac{(\lambda_B \varepsilon_1)^m}{m!} - A_1 \sum_{i=0}^{m-1} \frac{\lambda_F^i}{i! A_2^{i+m}} \left(\Gamma(i+m) - \frac{(A_2 \varepsilon_1)^{i+m}}{i+m} \right).
\end{aligned}$$

Proof: Please refer to Appendix B.

Due to $\varepsilon_1 \rightarrow 0$, $\varepsilon_2 \rightarrow 0$, $\varepsilon_4 \rightarrow 0$, $\varepsilon_5 \rightarrow 0$ when $\rho \rightarrow \infty$, we have $T_0^\infty \rightarrow 0$, $T_{11}^\infty \rightarrow 0$, $T_{12a}^\infty \rightarrow 0$, $T_{12b}^\infty \approx 1 - A_1 \sum_{i=0}^{m-1} \frac{\lambda_F^i \Gamma(i+m)}{i! A_2^{i+m}}$, which is a constant independent of ρ .

Remark 3. According to the results presented in Corollary 1, one can realize there is an OP floor when $\Theta_{th} > 1 + \frac{1}{\Theta_B - 1}$.

Utilizing $G_d = -\lim_{\rho \rightarrow \infty} \frac{\log P_{\text{out}}^{\text{DPA}}(\rho)}{\log \rho}$, the diversity order with the SGF scheme is obtained as

$$G_d^{\text{FPA}} = \begin{cases} m, & \Theta_{th} < \frac{\Theta_B}{\Theta_B - 1} \\ 0, & \Theta_{th} > \frac{\Theta_B}{\Theta_B - 1} \end{cases} \quad (17)$$

IV. OUTAGE PERFORMANCE ANALYSIS WITH DYNAMIC POWER ALLOCATION

In this section, a DPA scheme is proposed to avoid the OP floor and the analytical expression for the OP with the DPA scheme is derived.

A. Proposed dynamic power allocation scheme

In the previous analysis, D_B is always allocated to a fixed power ω that just gives priority to meet its QoS requirement, while the other power is allocated to D_F . One can observe from Corollary 1 that there is OP floor when $\Theta_{th} > 1 + \frac{1}{\Theta_B - 1}$. Recalling when $G_F > G_B$, D_B 's signal can be decoded firstly at D_F and the achievable rate of D_F is expressed as $R_F^1 = \log_2(1 + \rho \omega G_F)$. If $G_F < G_B$, D_F has not enough capacity to decode D_B 's signal at the first stage of SIC, the achievable rate of D_F is expressed as $R_F^2 = \log_2\left(1 + \frac{\rho \omega G_F}{1 + \rho \omega G_F}\right)$. It must be noted that in the scenarios wherein $G_F < G_B$, U can increase ω to ω_2 to make sure that D_F can decode D_B 's signal at the first stage of SIC, then the achievable rate will be changed from $R_F^2 = \log_2\left(1 + \frac{\rho \omega G_F}{1 + \rho \omega G_F}\right)$ to $R_F^3 = \log_2(1 + \rho \omega_2 G_F)$, where $\bar{\omega}_2 = 1 - \omega_2$ and $\omega_2 = 1 - \frac{\rho G_F - (\Theta_B - 1)}{\rho \Theta_B G_F}$. The goal of the DPA scheme is to maximize D_F 's achievable rate. Hence, the power allocation coefficient must be chosen according to the relationship between R_F^2 and R_F^3 . Specifically, if $R_F^2 > R_F^3$, the power allocation coefficient for D_B is ω otherwise ω_2 . Due to $R_F^2 < R_F^3 \Leftrightarrow \frac{\Theta_B G_B}{\rho G_B + 1} < G_F < G_B$, the achievable rate of D_F with the DPA scheme is expressed as

$$R_F = \begin{cases} R_F^1, & G_F > G_B \\ R_F^2, & G_F < \frac{\Theta_B G_B}{\rho G_B + 1} \\ R_F^3, & \frac{\Theta_B G_B}{\rho G_B + 1} < G_F < G_B \end{cases} \quad (18)$$

B. Outage performance analysis with dynamic power allocation scheme

On the ground of (18), the OP with the DPA scheme is expressed as (19), shown at the top of the this page, where T_0 and T_{11} are given in Theorem 1, T_2 denotes D_F 's signal that is decoded at the first stage when power allocation coefficient is ω , and T_3 denotes D_F 's signal that is decoded at the second stage when power allocation coefficient is ω_2 .

The following theorem provides the analytical expression for the OP of D_F with the DPA scheme.

Theorem 2. The OP of D_F with the DPA scheme, P_{out}^{dp} is expressed as

$$P_{out}^{DPA} = \begin{cases} T_0 + T_{11} + T_{2a}^a + T_3, & \Theta_B > \frac{1}{\Theta_{th}-1} \\ T_0 + T_{11} + T_{2a}^b + T_3, & \Theta_B < \frac{1}{\Theta_{th}-1} \end{cases} \quad (20)$$

where $T_{2a}^a = \bar{F}_{G_B}(\varepsilon_1) - A_1\Phi_5$, $T_{2a}^b = \bar{F}_{G_B}(\varepsilon_1) - A_1g_1\left(-\frac{1}{\rho}, \frac{\Theta_B}{\rho}, \varepsilon_1, \varepsilon_3\right) - A_1g_1(\varepsilon_3, \varepsilon_4, \varepsilon_3, \varepsilon_6) - A_1g_2\left(-\frac{1}{\rho}, \frac{\Theta_B}{\rho}, \varepsilon_6\right)$, $T_3 = A_1\Phi_5 - \bar{F}_{G_F}(\varepsilon_0)\bar{F}_{G_B}(\varepsilon_0) - A_1\sum_{i=0}^{m-1}\frac{(\lambda_F)^i\Phi_2}{i!}$, $\Phi_5 = g_2\left(-\frac{1}{\rho}, \frac{\Theta_B}{\rho}, \varepsilon_1\right)$, and $\Phi_6 = \frac{\Upsilon(i+m, A_2\varepsilon_0) - \Upsilon(i+m, A_2\varepsilon_1)}{A_2^{i+m}}$.

Proof: Please refer to Appendix C.

Eq. (20) provides an exact relationship between the OP of D_F with the DPA scheme and the system parameters. In addition to the insights mentioned in Theorem 1, an interesting phenomenon can be found. Intuitively, increasing the transmit power of D_B tends to stronger inter-user interference on D_F , which deteriorates the performance of D_F . However, in the DPA scheme, under some conditions, appropriately increasing the transmit power of D_B ensures the signal of D_B can be decoded successfully on D_F . The achievable rate of D_F can be enhanced through the SIC technique; thus the performance is improved. Similar to [17] and [22], the collaboration among the GB and GF users not only improves resource utilization, but also enhances the GF users' performance while not affecting the GB's QoS.

To obtain more insights, we derive the analytical expressions for the asymptotic OP of D_F with the DPA scheme.

Corollary 2. When $\rho \rightarrow \infty$, the asymptotic OP of D_F is expressed as (21), shown at the top of this page, where $T_{2b}^\infty = \frac{1}{m!}\left(\frac{\lambda_F\Theta_B}{\rho}\right)^m\left(1 - \frac{(\varepsilon_1\lambda_B)^m}{m!}\right)$, $T_3^\infty \approx \frac{\lambda_B^m(\varepsilon_0^m - \varepsilon_1^m)}{m!} + \frac{\lambda_F^m}{m!}\left(\varepsilon_0^m - \frac{\Theta_B}{\rho^m}\right) - A_1\sum_{i=0}^{m-1}\frac{\lambda_F^i\Phi_2^i}{i!}$, and $\Phi_2^\infty = \frac{\varepsilon_0^{i+m} - \varepsilon_1^{i+m}}{i+m}$.

Proof: Please refer to Appendix D.

Because of $T_0^\infty \propto \rho^{-m}$, $T_{11}^\infty \propto \rho^{-m}$, $T_{2b}^\infty \propto \rho^{-m}$, $T_3^\infty \propto \rho^{-m}$, we obtain $P_{out}^{DPA, \infty} \propto \rho^{-m}$.

Remark 4. It can be realized from Corollary 2 that OP floors can be avoided when DPA scheme is adopted.

Similar to (17), the diversity order with DPA scheme is obtained as

$$G_d^{DPA} = m \quad (22)$$

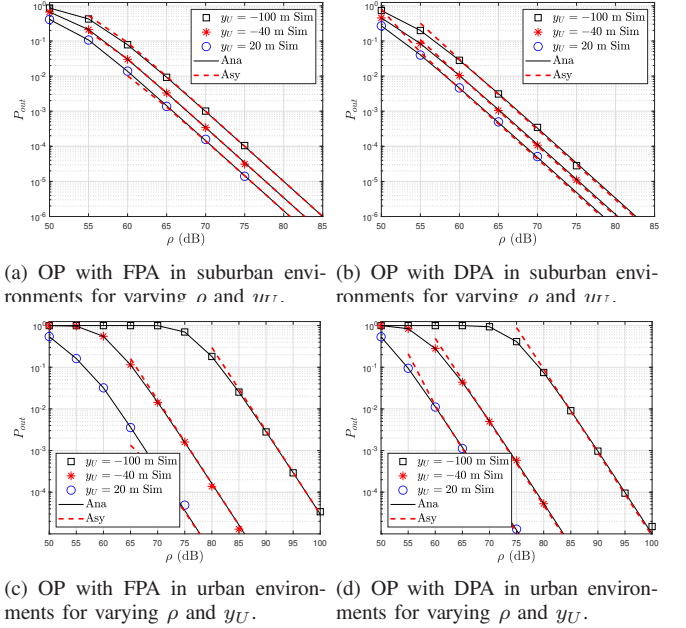


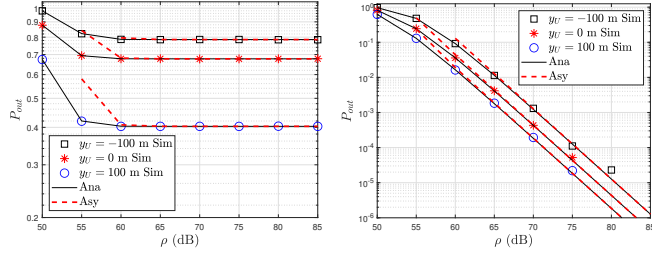
Fig. 2: The effect of UAV's position and ρ on the OP of D_F with $\Theta_{th} < 1 + \frac{1}{\Theta_B-1}$.

V. NUMERICAL RESULTS

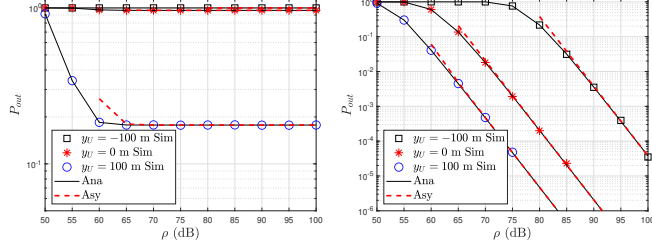
In this section, Monte-Carlo simulations are presented to prove our analysis on the outage performance of the aerial SGF NOMA system by varying the parameters, such as transmit SNR and power allocation coefficient. The main parameters are set as $m = 2$, $R_{th}^B = 0.2$ bps/Hz, $R_{th}^F = 2$ bps/Hz, $(x_B, y_B) = (50, -50)$, $(x_F, y_F) = (50, 50)$, and $(x_U, y_U, z_U) = (0, 0, 100)$, unless stated otherwise. In all the figures, 'Sim', 'Ana', and 'Asy' denote the simulation, numerical, and asymptotic results, respectively.

Fig. 2 presents the effect of UAV's position and ρ on the OP of D_F when $\Theta_{th} < 1 + \frac{1}{\Theta_B-1}$. It can be observed that OP is improved with the increase of transmission SNR. At the same time, by comparing Fig. 2(a) and Fig. 2(b), it can also be observed that the curve of GF user's OP with DPA is always below the user OP curve with FPA, which demonstrates that the designed DPA scheme can effectively enhance the outage performance. By comparing Fig. 2(a) and Fig. 2(c), it can be observed that the outage performance of D_F in suburban environments outperforms that in urban environments because there is a high LoS probability due to fewer shelters in suburban environments, which leads to a lower attenuation with minor average path loss. Thus, the degradation due to the variation of elevation angle is much severe in urban environment. The same conclusion can also be found by comparing Fig. 2(c) and Fig. 2(d), and Fig. 2(b) and Fig. 2(d).

Fig. 3 demonstrates the effect of UAV's position and the transmission SNR on the OP of D_F when $\Theta_{th} > 1 + \frac{1}{\Theta_B-1}$. It can be observed from Fig. 3(a) and Fig. 3(c) that the OP deteriorates as ρ decreases at lower- ρ region. However, there is a floor for OP, which denotes that the OP gradually approaches a constant at the higher- ρ region. This is because the base



(a) OP with FPA in suburban environments for varying ρ and y_U . (b) OP with DPA in suburban environments for varying ρ and y_U .



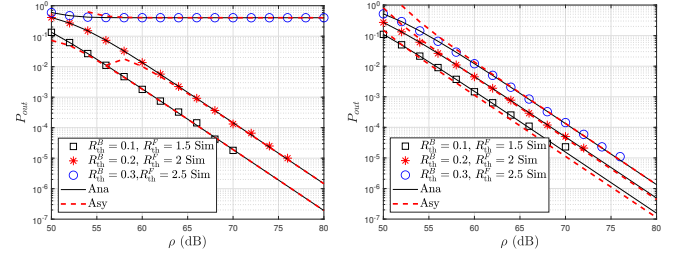
(c) OP with FPA in urban environments for varying ρ and y_U . (d) OP with DPA in urban environments for varying ρ and y_U .

Fig. 3: The effect of UAV's position and ρ on the OP of D_F with $\Theta_{th} > 1 + \frac{1}{\Theta_B - 1}$.

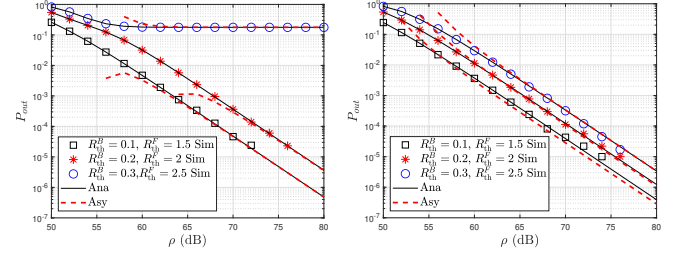
station needs to allocate more power to D_B , resulting in too much interference on D_F . When the signals for D_B cannot be decoded on D_F with increasing transmit SNR, the SINR at D_F tends to a constant, which is independent of ρ . As shown in Fig. 3(b) and Fig. 3(d), one can also observe that the outage performance with the DPA scheme outperforms that with the FPA scheme. Moreover, it can be found that the outage performance of D_F in the DPA scheme will also improve with the increase of ρ in the case of high- ρ region. Specifically, the OP floor problem is solved by the DPA scheme. The reason is that more power allocated to D_B ensures that D_F can decode the signal of D_B successfully. With the SIC technology, the inter-user interference is deleted and the achievable rate of D_F is improved, thereby the performance is enhanced.

Furthermore, it can be seen in Figs. 2 and 3 that OP is improved as the distance between U and D_F decreases. The reason is given as follows. Compared with the probability of loss propagation, the main factor on OP is path loss, which decreases with distance.

Fig. 4 demonstrates the impact of RRT of D_B and D_F on the OP of D_F . It can be observed that the larger the R_{th}^B and R_{th}^F , the larger the OP, which is easy to follow because larger RRT denotes higher requirement. As demonstrated in Fig. 4(a) and Fig. 4(c), it can be observed that the relationship between the RRT for D_B and D_F under the condition in which the resources can be shared also significantly affects the OP of D_F , which is testified in Theorem 1. Furthermore, the results in Fig. 4(b) and Fig. 4(d) verify that the DPA scheme solves the OP floors perfectly. Then, the effectiveness of the DPA scheme is testified. It must be noted that the power allocation in the DPA scheme not only depends on the global CSI but also on the RRT of D_B , which is expressed in Eq. (18). Thus, jointly designing the RRT of D_B and D_F based on the global CSI

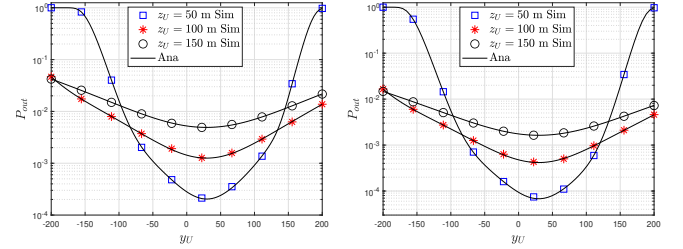


(a) OP with FPA in suburban environments for varying ρ , R_{th}^B , and R_{th}^F . (b) OP with DPA in suburban environments for varying ρ , R_{th}^B , and R_{th}^F .

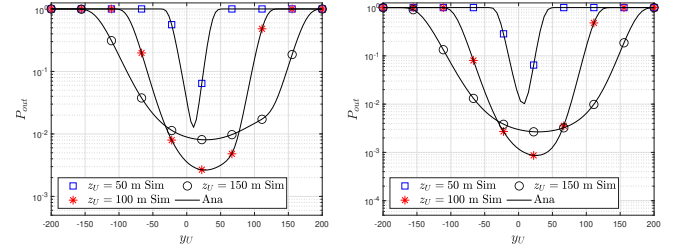


(c) OP with FPA in urban environments for varying ρ , R_{th}^B , and R_{th}^F . (d) OP with DPA in urban environments for varying ρ , R_{th}^B , and R_{th}^F .

Fig. 4: The impact of RRT of D_B and D_F on the OP of D_F .



(a) OP with FPA in suburban environments for varying y_U and z_U . (b) OP with DPA in suburban environments for varying y_U and z_U .



(c) OP with FPA in urban environments for varying y_U and z_U . (d) OP with DPA in urban environments for varying y_U and z_U .

Fig. 5: The impact of the UAV's position and altitude on the OP of D_F with $R_{th}^B = 0.2$ and $R_{th}^F = 2$.

can maximize the achievable rate of GF users while ensuring the QoS of the GB user, which will be part of future work.

Figs. 5 and 6 demonstrate the impact of the UAV's position and altitude on the OP of the GF user with varying RRT requirements. One can observe that the OP first decreases and then increases, which means there is an optimal location for the UAV so that the GF user can obtain the optimal performance. At the same time, it can be observed that under different environments and power allocation schemes, the 3D location of the UAV has different effects on the OP. This is be-

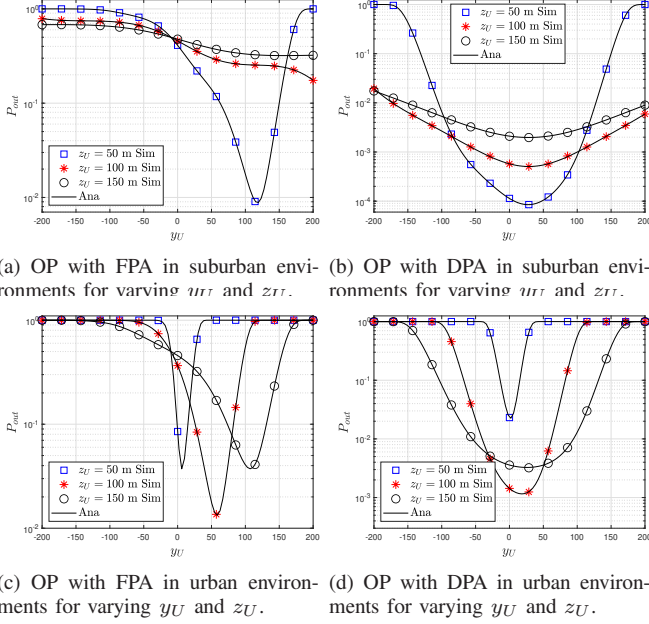


Fig. 6: The impact of the UAV's position and altitude on the OP of D_F with $R_{th}^B = 0.5$ and $R_{th}^F = 2.5$.

cause the trade-off between the probability of LoS propagation and the path loss caused by long-distance communication are different. Comparing Fig. 5 and Fig. 6, it can be observed that the OP with the DPA scheme outperforms that with the FPA scheme. The result in Fig. 5(a) and Fig. 6(a) demonstrates that the relationship between the RRT for D_B and D_F makes a big difference to the OP of D_F in suburban environments with the FPA scheme. The same conclusion can also be observed by comparing Fig. 5(c) and Fig. 6(c). However, the effect of the relationship between the RRT for D_B and D_F makes little difference to the OP of D_F in the same environments with the DPA scheme, which is found by comparing Fig. 5(b) and Fig. 6(b), and Fig. 5(d) and Fig. 6(d). The reason is that the CSI of D_F is also considered in the DPA scheme, which is expressed in Eq. (18).

VI. CONCLUSIONS

This work analyzed the outage performance of an aerial SGF NOMA system. Firstly, the outage performance of UAV-enabled downlink NOMA systems was analyzed with the SGF transmission scheme. The exact and asymptotic expressions for the OP of the GF user under the FPA scheme were derived. It was found that there are OP floors under stringent conditions on quality of service requirements. A DPA scheme was proposed to eliminate the OP floor at the high-SNR region. The analytical expressions for the exact and asymptotic OP of the GF user were derived applicable to this later scheme. Numerical and simulation results demonstrate that the outage performance of the GF user was improved by utilizing the proposed DPA scheme. And the effects of system parameters, such as UAV location and altitude, on the outage performance were analyzed. It was observed that there is an optimal position for the UAV to minimize D_F 's OP. The optimal placement

is related to the environment, the altitude of the UAV, and the transmission SNR. Optimizing the outage performance of the GF user by designing the trajectory of the UAV will be conducted as part of our future work.

ACKNOWLEDGEMENTS

This work was supported by the National Natural Science Foundation of China under Grant 61971080 and the Open Fund of the Shaanxi Key Laboratory of Information Communication Network and Security under Grant ICNS201807. The authors would like to thank the editor for efficiently handling the review of this paper and the anonymous reviewers for their valuable suggestions and critical comments that helped to improve the quality of the paper.

APPENDIX A PROOF OF THEOREM 1

Based on (4), we obtain $T_0 = F_{GB}(\varepsilon_1)$. On the ground of (13), T_1 is expressed as

$$T_1 = \underbrace{\Pr \{G_B > \varepsilon_1, G_F > G_B, R_F^1 < R_{th}^F\}}_{T_{11}} + \underbrace{\Pr \{G_B > \varepsilon_1, G_F < G_B, R_F^2 < R_{th}^F\}}_{T_{12}} \quad (23)$$

where T_{11} denotes D_F 's signal is decoded at the first stage of SIC and T_{12} denotes D_F 's signal is decoded at the second stage of SIC. From (7) and (11), we have

$$\begin{aligned} & \Pr \{ \log_2(1 + \bar{\omega}\rho G_F) < R_{th}^F \} \\ &= \Pr \left\{ G_F < \frac{\Theta_{th} - 1}{\bar{\omega}\rho} \right\} \\ &= \Pr \left\{ G_F < \frac{\varepsilon_2 G_B}{G_B - \varepsilon_1} \right\} \end{aligned} \quad (24)$$

where $\Theta_{th} = 2^{R_{th}^F}$, $\varepsilon_2 = \frac{\Theta_B(\Theta_{th}-1)}{\rho}$, and $\Theta_B = 2^{R_{th}^B}$. Then, grounded on (4) and (5), T_{11} is expressed as

$$\begin{aligned} T_{11} &= \Pr \left\{ G_B > \varepsilon_1, G_F > G_B, G_F < \frac{\varepsilon_2 G_B}{G_B - \varepsilon_1} \right\} \\ &= \Pr \left\{ G_B > \varepsilon_1, G_B < G_F < \frac{\varepsilon_2 G_B}{G_B - \varepsilon_1}, \right. \\ &\quad \left. G_B < \frac{\varepsilon_2 G_B}{G_B - \varepsilon_1} \right\} \\ &= \Pr \left\{ G_B < G_F < \frac{\varepsilon_2 G_B}{G_B - \varepsilon_1}, \varepsilon_1 < G_B < \varepsilon_0 \right\} \\ &= \Pr \left\{ G_F < \frac{\varepsilon_2 G_B}{G_B - \varepsilon_1}, \varepsilon_1 < G_B < \varepsilon_0 \right\} \\ &\stackrel{\triangle}{=} \chi_1 \\ &\quad - \underbrace{\Pr \{G_B < G_F, \varepsilon_1 < G_B < \varepsilon_0\}}_{\triangleq \chi_2} \end{aligned} \quad (25)$$

where $\varepsilon_0 = \varepsilon_1 + \varepsilon_2 = \frac{\Theta_B \Theta_{th} - 1}{\rho}$ and χ_1 is expressed as

$$\begin{aligned}\chi_1 &= \Pr \left\{ G_F < \frac{\varepsilon_2 G_B}{G_B - \varepsilon_1}, \varepsilon_1 < G_B < \varepsilon_0 \right\} \\ &= \int_{\varepsilon_1}^{\varepsilon_0} f_{G_B}(x) F_{G_F} \left(\frac{\varepsilon_2 x}{x - \varepsilon_1} \right) dx \\ &= F_{G_B}(\varepsilon_0) - F_{G_B}(\varepsilon_1) - A_1 \Phi_1\end{aligned}\quad (26)$$

where $A_1 = \frac{\lambda_B^m}{\Gamma(m)}$ and $\Phi_1 = \sum_{i=0}^{m-1} \frac{\lambda_F^i}{i!} \int_{\varepsilon_1}^{\varepsilon_0} y^{m-1} \left(\frac{\varepsilon_2 y}{y - \varepsilon_1} \right)^i e^{-\lambda_B y - \frac{\lambda_F \varepsilon_2 y}{y - \varepsilon_1}} dy$. To the authors' best knowledge, it is very difficult to obtain the closed-form expression of Φ_1 . To facilitate the following analysis, we define

$$g_1(a, b, s, t) = \sum_{i=0}^{m-1} \frac{(\lambda_F b)^i}{i!} \int_s^t \frac{y^{m+i-1}}{(y-a)^i} e^{-\lambda_B y - \frac{b \lambda_F y}{y-a}} dy \quad (27)$$

Utilizing Gaussian-Chebyshev quadrature [31, (25.4.39)], we obtain the approximation for $g_1(a, b, s, t)$ as

$$\begin{aligned}g_1(a, b, s, t) &= \frac{\pi}{N} \sum_{i=0}^{m-1} \frac{(\lambda_F b)^i}{i!} \sum_{n=1}^N \frac{(\mu_n(s, t))^{m+i-1}}{(\mu_n(s, t) - a)^i} \\ &\quad \times e^{-\lambda_B \mu_n(s, t) - \frac{\lambda_F b \mu_n(s, t)}{\mu_n(s, t) - a}} \\ &\quad \times \sqrt{(\mu_n(s, t) - s)(t - \mu_n(s, t))}\end{aligned}\quad (28)$$

where $\mu_n(s, t) = \frac{t+s}{2} + \frac{(t-s)\tau_n}{2}$, $\tau_n = \cos \frac{(2n-1)\pi}{2N}$, and N is the summation terms, which reflects accuracy vs. complexity. Then, we obtain $\Phi_1 = g_1(\varepsilon_1, \varepsilon_2, \varepsilon_1, \varepsilon_0)$.

Utilizing [30, (3.351.1)], χ_2 is obtained as

$$\begin{aligned}\chi_2 &= \Pr \{ G_B < G_F, \varepsilon_1 < G_B < \varepsilon_0 \} \\ &= \int_{\varepsilon_1}^{\varepsilon_0} f_{G_B}(y) F_{G_F}(y) dy \\ &= F_{G_B}(\varepsilon_0) - F_{G_B}(\varepsilon_1) - \frac{\lambda_B^m}{\Gamma(m)} \sum_{i=0}^{m-1} \frac{\lambda_F^i}{i!} \\ &\quad \int_{\varepsilon_1}^{\varepsilon_0} e^{-(\lambda_B + \lambda_F)y} y^{m+i-1} dy \\ &= F_{G_B}(\varepsilon_0) - F_{G_B}(\varepsilon_1) - A_1 \sum_{i=0}^{m-1} \frac{\lambda_F^i \Phi_2}{i!}\end{aligned}\quad (29)$$

where $A_2 = \lambda_B + \lambda_F$, $\Phi_2 = \frac{\Upsilon(i+m, A_2 \varepsilon_0) - \Upsilon(i+m, A_2 \varepsilon_1)}{A_2^{i+m}}$, and $\Upsilon(\cdot, \cdot)$ is lower incomplete Gamma function as defined by [30, (8.350.2)].

Similar to T_{11} , T_{12} is expressed as

$$\begin{aligned}T_{12} &= \Pr \{ G_B > \varepsilon_1, G_F < G_B, \\ &\quad \log_2 \left(1 + \frac{\bar{\omega} \rho G_F}{1 + \rho \omega G_F} \right) < R_{th}^F \} \\ &= \Pr \{ G_B > \varepsilon_1, G_F < G_B, \\ &\quad \rho(1 - \Theta_{th} \omega) G_F < \Theta_{th} - 1 \}\end{aligned}\quad (30)$$

Since there is

$$\begin{aligned}\Pr \{ \rho(1 - \Theta_{th} \omega) G_F < \Theta_{th} - 1 \} &= \Pr \{ 1 - \Theta_{th} \omega < 0 \} \\ &+ \Pr \left\{ G_F < \frac{\varepsilon_4 G_B}{G_B - \varepsilon_3}, 1 - \Theta_{th} \omega > 0 \right\}\end{aligned}\quad (31)$$

where $\varepsilon_3 = \frac{\Theta_B - 1}{\rho} \frac{\Theta_{th}}{\Theta_{th} - (\Theta_{th} - 1)\Theta_B} = \varepsilon_1 \frac{\Theta_{th}}{\Theta_{th} - (\Theta_{th} - 1)\Theta_B} > \varepsilon_1$ and $\varepsilon_4 = \frac{\Theta_B(\Theta_{th} - 1)}{(\Theta_B - \Theta_{th}(\Theta_B - 1))\rho}$. Furthermore, we obtain the following result

$$\begin{aligned}\Pr \{ 1 - \omega \Theta_{th} < 0 \} \\ &= \Pr \left\{ 1 - \frac{\rho \Theta_B G_B - \rho G_B + \Theta_B - 1}{\rho \Theta_B G_B} \Theta_{th} < 0 \right\} \\ &= \Pr \left\{ \rho \left(\frac{\Theta_B}{\Theta_B - 1} - \Theta_{th} \right) G_B < \Theta_{th} \right\}\end{aligned}\quad (32)$$

Thus, the relationship between Θ_{th} and $\frac{\Theta_B}{\Theta_B - 1}$ must be considered first.

1) When $\Theta_{th} < \frac{\Theta_B}{\Theta_B - 1}$, we have

$$\Pr \{ 1 - \omega \Theta_{th} < 0 \} = \Pr \{ G_B < \varepsilon_3 \} \quad (33)$$

Thus, we have

$$\begin{aligned}\Pr \{ \rho(1 - \Theta_{th} \omega) G_F < \Theta_{th} - 1 \} \\ &= \Pr \{ G_B < \varepsilon_3 \} \\ &+ \Pr \left\{ G_F < \frac{\varepsilon_4 G_B}{G_B - \varepsilon_3}, G_B > \varepsilon_3 \right\}\end{aligned}\quad (34)$$

Substituting (34) into (30), we have

$$\begin{aligned}T_{12a} &= \Pr \{ G_F < G_B, \varepsilon_1 < G_B < \varepsilon_3 \} \\ &+ \Pr \left\{ G_B > \varepsilon_3, G_F < \min \left(G_B, \frac{\varepsilon_4 G_B}{G_B - \varepsilon_3} \right) \right\}\end{aligned}\quad (35)$$

The 2nd term in (35) is derived as

$$\begin{aligned}\Pr \left\{ G_B > \varepsilon_3, G_F < \min \left(G_B, \frac{\varepsilon_4 G_B}{G_B - \varepsilon_3} \right) \right\} \\ &= \Pr \left\{ G_B > \varepsilon_3, G_F < G_B, G_B < \frac{\varepsilon_4 G_B}{G_B - \varepsilon_3} \right\} \\ &+ \Pr \left\{ G_B > \varepsilon_3, G_F < \frac{\varepsilon_4 G_B}{G_B - \varepsilon_3}, G_B > \frac{\varepsilon_4 G_B}{G_B - \varepsilon_3} \right\} \\ &= \Pr \{ G_B > \varepsilon_3, G_F < G_B, G_B < \varepsilon_5 \} \\ &+ \Pr \left\{ G_B > \varepsilon_3, G_F < \frac{\varepsilon_4 G_B}{G_B - \varepsilon_3}, G_B > \varepsilon_5 \right\}\end{aligned}\quad (36)$$

where $\varepsilon_5 = \varepsilon_3 + \varepsilon_4 = \frac{2\Theta_B \Theta_{th} - \Theta_{th} - \Theta_B}{\rho(\Theta_{th} + \Theta_B - \Theta_{th} \Theta_B)}$. Then, T_{12a} is expressed as

$$\begin{aligned}T_{12a} &= \Pr \{ G_F < G_B, \varepsilon_1 < G_B < \varepsilon_3 \} \\ &+ \Pr \{ G_F < G_B, \varepsilon_3 < G_B < \varepsilon_5 \} \\ &+ \Pr \left\{ G_F < \frac{\varepsilon_4 G_B}{G_B - \varepsilon_3}, G_B > \varepsilon_3, G_B > \varepsilon_5 \right\} \\ &= \underbrace{\Pr \{ G_F < G_B, \varepsilon_1 < G_B < \varepsilon_5 \}}_{\triangleq \chi_3} \\ &+ \underbrace{\Pr \left\{ G_F < \frac{\varepsilon_4 G_B}{G_B - \varepsilon_3}, G_B > \varepsilon_5 \right\}}_{\triangleq \chi_4}\end{aligned}\quad (37)$$

With the same method as (29), we obtain

$$\chi_3 = F_{G_B}(\varepsilon_5) - F_{G_B}(\varepsilon_1) - A_1 \sum_{i=0}^{m-1} \frac{\lambda_F^i \Phi_3}{i!} \quad (38)$$

where $\Phi_3 = \frac{\Upsilon(i+m, A_2 \varepsilon_5) - \Upsilon(i+m, A_2 \varepsilon_1)}{A_2^{i+m}}$. With the similar method as (26), χ_4 is obtained as

$$\begin{aligned} \chi_4 &= \Pr \left\{ G_F < \frac{\varepsilon_4 G_B}{G_B - \varepsilon_3}, G_B > \varepsilon_5 \right\} \\ &= \int_{\varepsilon_5}^{\infty} f_{G_B}(y) F_{G_F} \left(\frac{\varepsilon_4 y}{y - \varepsilon_3} \right) dy \\ &= \bar{F}_{G_B}(\varepsilon_5) - A_1 \Phi_4 \end{aligned} \quad (39)$$

where $\bar{F}_{G_X}(x) = 1 - F_{G_X}(x)$ and $\Phi_4 = \sum_{i=0}^{m-1} \frac{(\lambda_F \varepsilon_4)^i}{i!} \int_{\varepsilon_5}^{\infty} e^{-\lambda_B y - \frac{\lambda_F \varepsilon_4 y}{y - \varepsilon_3}} \frac{y^{m+i-1}}{(y - \varepsilon_3)^i} dy$. To facilitate the following analysis, we define

$$g_2(a, b, c) = \sum_{i=0}^{m-1} \frac{(\lambda_F b)^i}{i!} \int_c^{\infty} e^{-\lambda_B y - \frac{b \lambda_F y}{y-a}} \frac{y^{m+i-1}}{(y-a)^i} dy \quad (40)$$

Utilizing Gaussian-Chebyshev quadrature [31, (25.4.39)], we obtain the approximation for $g_2(a, b, c)$ as

$$\begin{aligned} g_2(a, b, c) &= \sum_{i=0}^{m-1} \frac{(\lambda_F b)^i}{i!} \sum_{n=1}^N w_n e^{\iota_n - (\lambda_B \iota_n + \frac{\lambda_F b \iota_n}{\iota_n - a})} \frac{\iota_n^{m+i-1}}{(\iota_n - a)^i} \\ &\quad - \sum_{i=0}^{m-1} \frac{(\lambda_F b)^i \pi}{i! N} \sum_{n=1}^N e^{-(\lambda_B \mu_n(0, c) + \frac{\lambda_F b \mu_n(0, c)}{\mu_n(0, c) - a})} \\ &\quad \times \frac{(\mu_n(0, c))^{m+i-1} \sqrt{\mu_n(0, c)(c - \mu_n(0, c))}}{(\mu_n(0, c) - a)^i} \end{aligned} \quad (41)$$

where ι_n is the n th zeros of Laguerre polynomials and w_n is the Gaussian weight, which are given in Table (25.9) of [31]. Then, we obtain $\Phi_4 = g_2(\varepsilon_3, \varepsilon_4, \varepsilon_5)$.

2) When $\Theta_{th} > \frac{\Theta_B}{\Theta_B - 1}$, due to $\Pr \{1 - \omega \Theta_{th} < 0\} = 1$, we obtain

$$\begin{aligned} T_{12b} &= \Pr \{G_F < G_B, G_B > \varepsilon_1\} \\ &= \int_{\varepsilon_1}^{\infty} f_{G_B}(y) F_{G_F}(y) dy \\ &= \bar{F}_{G_B}(\varepsilon_1) - \frac{\lambda_B^m}{\Gamma(m)} \sum_{i=0}^{m-1} \frac{\lambda_F^i}{i!} \int_{\varepsilon_1}^{\infty} y^{m+i-1} e^{-(\lambda_B + \lambda_F)y} dy \\ &= \bar{F}_{G_B}(\varepsilon_1) - A_1 \sum_{i=0}^{m-1} \frac{\lambda_F^i \Gamma(i+m, A_2 \varepsilon_1)}{i! A_2^{i+m}} \end{aligned} \quad (42)$$

where $\Gamma(\cdot, \cdot)$ is upper incomplete Gamma function, which is defined by [30, (3.351.2)].

APPENDIX B PROOF OF COROLLARY 1

Utilizing $e^x = \sum_{j=0}^{\infty} \frac{x^j}{j!}$, we obtain $\sum_{j=0}^{n-1} \frac{x^j}{j!} = e^x - \frac{x^n}{n!} + O(x^n)$, then we have $F_{G_X}(x) \rightarrow \frac{(\lambda_X x)^m}{m!}$ when $x \rightarrow 0$. Thus, we have $T_0^\infty = F_{G_B}^\infty(\varepsilon_1) = \frac{(\lambda_B \varepsilon_1)^m}{m!}$.

When $\rho \rightarrow \infty$, we have $\varepsilon_1 \rightarrow 0$, $\varepsilon_2 \rightarrow 0$, $\varepsilon_3 \rightarrow 0$, $\varepsilon_4 \rightarrow 0$, and $\frac{\varepsilon_2 G_B}{G_B - \varepsilon_1} \rightarrow \varepsilon_2$, by utilizing $\Upsilon(n, x) \stackrel{x \rightarrow 0}{\approx} \frac{x^n}{n}$, T_{11}^∞ is obtained as

$$\begin{aligned} T_{11}^\infty &= \Pr \{G_B < G_F < \varepsilon_2, \varepsilon_1 < G_B < \varepsilon_0\} \\ &= \int_{\varepsilon_1}^{\varepsilon_0} f_{G_B}(y) (F_{G_F}^\infty(\varepsilon_2) - F_{G_F}(y)) dy \\ &= \int_{\varepsilon_1}^{\varepsilon_0} f_{G_B}(y) \frac{\lambda_F^m \varepsilon_2^m}{m!} dy \\ &\quad - \int_{\varepsilon_1}^{\varepsilon_0} f_{G_B}(y) \left(1 - e^{-\lambda_F y} \sum_{i=0}^{m-1} \frac{\lambda_F^i y^i}{i!} \right) dy \\ &= \left(\frac{(\lambda_F \varepsilon_2)^m}{m!} - 1 \right) \int_{\varepsilon_1}^{\varepsilon_0} f_{G_B}(y) dy \\ &\quad + \frac{\lambda_B^m}{\Gamma(m)} \sum_{i=0}^{m-1} \frac{\lambda_F^i}{i!} \int_{\varepsilon_1}^{\varepsilon_0} y^{m+i-1} e^{-(\lambda_B + \lambda_F)y} dy \\ &\approx \frac{\lambda_B^m (\varepsilon_0^m - \varepsilon_1^m)}{m!} \left(\frac{(\lambda_F \varepsilon_2)^m}{m!} - 1 \right) \\ &\quad + \frac{\lambda_B^m}{\Gamma(m)} \sum_{i=0}^{m-1} \frac{\lambda_F^i (\varepsilon_0^{i+m} - \varepsilon_1^{i+m})}{i! (i+m)} \end{aligned} \quad (43)$$

Similarly, due to $\frac{\varepsilon_4 G_B}{G_B - \varepsilon_3} \rightarrow \varepsilon_4$, T_{12a}^∞ is obtained as

$$T_{12a}^\infty = \chi_3^\infty + \chi_4^\infty \quad (44)$$

where

$$\begin{aligned} \chi_3^\infty &= \Pr \{G_F < G_B, \varepsilon_1 < G_B < \varepsilon_5\} \\ &= \int_{\varepsilon_1}^{\varepsilon_5} f_{G_B}(y) F_{G_F}(y) dy \\ &= \int_{\varepsilon_1}^{\varepsilon_5} f_{G_B}(y) \left(1 - e^{-\lambda_F y} \sum_{i=0}^{m-1} \frac{\lambda_F^i y^i}{i!} \right) dy \\ &\approx \frac{\lambda_B^m (\varepsilon_5^m - \varepsilon_1^m)}{m!} - A_1 \sum_{i=0}^{m-1} \frac{\lambda_F^i (\varepsilon_5^{i+m} - \varepsilon_1^{i+m})}{i! (i+m)} \end{aligned} \quad (45)$$

and

$$\begin{aligned} \chi_4^\infty &= \Pr \{G_F < \varepsilon_4, G_B > \varepsilon_5\} \\ &= \int_{\varepsilon_5}^{\infty} f_B(y) F_{G_F}^\infty(\varepsilon_4) dy \\ &\approx \frac{(\lambda_F \varepsilon_4)^m}{m!} \left(1 - \frac{(\lambda_B \varepsilon_5)^m}{m!} \right) \end{aligned} \quad (46)$$

Similarly, on the ground of (42), T_{12b}^∞ is obtained as

$$\begin{aligned} T_{12b}^\infty &\approx 1 - \frac{(\lambda_B \varepsilon_1)^m}{m!} \\ &\quad - A_1 \sum_{i=0}^{m-1} \frac{\lambda_F^i}{i! A_2^{i+m}} \left(\Gamma(i+m) - \frac{(A_2 \varepsilon_1)^{i+m}}{i+m} \right) \end{aligned} \quad (47)$$

APPENDIX C PROOF OF THEOREM 2

T_0 and T_{11} are given in Theorem 1.

Substituting (12) into (19), T_2 is expressed as

$$\begin{aligned} T_2 &= \Pr \left\{ G_B > \varepsilon_1, G_F < \frac{\Theta_B G_B}{\rho G_B + 1}, \right. \\ &\quad \left. (1 - \Theta_{th} \omega) \rho G_F < \Theta_{th} - 1 \right\} \end{aligned} \quad (48)$$

1) When $\Theta_{th} < \frac{\Theta_B}{\Theta_B - 1}$, we obtain

$$\begin{aligned}
T_{2a} &= \Pr \left\{ G_B > \varepsilon_1, G_F < \frac{\Theta_B G_B}{\rho G_B + 1}, G_B < \varepsilon_3 \right\} \\
&\quad + \Pr \left\{ G_B > \varepsilon_1, G_F < \frac{\Theta_B G_B}{\rho G_B + 1}, \right. \\
&\quad \left. G_F < \frac{\varepsilon_4 G_B}{G_B - \varepsilon_3}, G_B > \varepsilon_3 \right\} \\
&= \Pr \left\{ G_F < \frac{\Theta_B G_B}{\rho G_B + 1}, \varepsilon_1 < G_B < \varepsilon_3 \right\} \\
&\quad \stackrel{\triangle}{=} \chi_5 \\
&\quad + \Pr \left\{ G_F < \min \left\{ \frac{\Theta_B G_B}{\rho G_B + 1}, \frac{\varepsilon_4 G_B}{G_B - \varepsilon_3} \right\}, G_B > \varepsilon_3 \right\} \\
&\quad \stackrel{\triangle}{=} \chi_6
\end{aligned} \tag{49}$$

Considering the relationship between $\frac{\Theta_B G_B}{\rho G_B + 1}$ and $\frac{\varepsilon_4 G_B}{G_B - \varepsilon_3}$, we obtain

$$\begin{aligned}
&\Pr \left\{ \frac{\varepsilon_4 G_B}{G_B - \varepsilon_3} - \frac{\Theta_B G_B}{\rho G_B + 1} > 0 \right\} \\
&= \begin{cases} 1, & \Theta_B > \frac{1}{\Theta_{th} - 1}, G_B > \varepsilon_3 \\ \Pr \{ G_B < \varepsilon_6 \}, & \Theta_B < \frac{1}{\Theta_{th} - 1}, G_B > \varepsilon_3 \end{cases} \tag{50}
\end{aligned}$$

where $\varepsilon_6 = \frac{\Theta_B \varepsilon_3 + \varepsilon_4}{\Theta_B (\Theta_B + 1 - \Theta_{th} \Theta_B)}$. Then, we obtain $\chi_6 = \Pr \left\{ G_F < \frac{\Theta_B G_B}{\rho G_B + 1}, G_B > \varepsilon_3 \right\}$ for $\Theta_B > \frac{1}{\Theta_{th} - 1}$. Thus, we obtain

$$\begin{aligned}
T_{2a}^a &= \Pr \left\{ G_F < \frac{\Theta_B G_B}{\rho G_B + 1}, \varepsilon_1 < G_B < \varepsilon_3 \right\} \\
&\quad + \Pr \left\{ G_F < \frac{\Theta_B G_B}{\rho G_B + 1}, G_B > \varepsilon_3 \right\} \\
&= \Pr \left\{ G_F < \frac{\Theta_B G_B}{\rho G_B + 1}, G_B > \varepsilon_1 \right\} \\
&= \int_{\varepsilon_1}^{\infty} f_{G_B}(y) F_{G_F} \left(\frac{\Theta_B y}{\rho y + 1} \right) dy \\
&= \bar{F}_{G_B}(\varepsilon_1) - A_1 g_2 \left(-\frac{1}{\rho}, \frac{\Theta_B}{\rho}, \varepsilon_1 \right)
\end{aligned} \tag{51}$$

For $\Theta_B < \frac{1}{\Theta_{th} - 1}$, we have

$$\begin{aligned}
\chi_6 &= \Pr \left\{ G_F < \frac{\Theta_B G_B}{\rho G_B + 1}, G_B > \varepsilon_3, G_B < \varepsilon_6 \right\} \\
&\quad + \Pr \left\{ G_F < \frac{\varepsilon_4 G_B}{G_B - \varepsilon_3}, G_B > \varepsilon_3, G_B > \varepsilon_6 \right\}
\end{aligned} \tag{52}$$

Due to $\varepsilon_6 - \varepsilon_3 = \frac{(\Theta_{th} - 1)\Theta_B \Theta_B \varepsilon_3 + \varepsilon_4}{\Theta_B (1 - (\Theta_{th} - 1)\Theta_B)} > 0$, we obtain (53), shown at the top of the the next page.

2) When $\Theta_{th} > \frac{\Theta_B}{\Theta_B - 1}$, we have

$$T_{2b} = \Pr \left\{ G_F < \frac{\Theta_B G_B}{\rho G_B + 1}, G_B > \varepsilon_1 \right\} = T_{2a}^a \tag{54}$$

With the similar method, T_3 is obtained as (55), shown at the top of the next page, where $\Phi_5 = g_2 \left(-\frac{1}{\rho}, \frac{\Theta_B}{\rho}, \varepsilon_1 \right)$.

APPENDIX D PROOF OF COROLLARY 2

When $\rho \rightarrow \infty$, we have $F_{G_F}^{\infty}(x) \rightarrow \frac{(\lambda_X x)^m}{m!}$, $\varepsilon_1 \rightarrow 0$, $\varepsilon_2 \rightarrow 0$, $\varepsilon_3 \rightarrow 0$, $\frac{\Theta_B G_B}{\rho G_B + 1} \rightarrow \frac{\Theta_B}{\rho}$, and $\omega \rightarrow 1 - \frac{1}{\Theta_B}$. For $\Theta_{th} > \frac{\Theta_B}{\Theta_B - 1}$, we have

$$\begin{aligned}
&\Pr \{ R_F^2 < R_{th}^F \} \\
&= \Pr \left\{ \log \left(1 + \frac{\rho \bar{\omega} G_F}{1 + \rho \omega G_F} \right) < R_{th}^F \right\} \\
&\approx 1
\end{aligned} \tag{56}$$

Thus, T_{2a}^{∞} and T_{2b}^{∞} are obtained as

$$T_{2a}^{\infty} = 0 \tag{57}$$

and

$$\begin{aligned}
T_{2b}^{\infty} &= \Pr \left\{ G_B > \varepsilon_1, G_F < \frac{\Theta_B}{\rho} \right\} \\
&= \frac{1}{m!} \left(\frac{\lambda_F \Theta_B}{\rho} \right)^m \left(1 - \frac{(\varepsilon_1 \lambda_B)^m}{m!} \right)
\end{aligned} \tag{58}$$

respectively.

Similarly, T_3^{∞} is obtained as

$$\begin{aligned}
T_3^{\infty} &= \Pr \left\{ \frac{\Theta_B}{\rho} < G_F < G_B, \varepsilon_1 < G_B < \varepsilon_0 \right\} \\
&\quad + \Pr \left\{ \frac{\Theta_B}{\rho} < G_F < \varepsilon_0, G_B > \varepsilon_0 \right\} \\
&= \int_{\varepsilon_1}^{\varepsilon_0} f_{G_B}(y) \left(F_{G_F}(y) - F_{G_F}^{\infty} \left(\frac{\Theta_B}{\rho} \right) \right) dy \\
&\quad + (1 - F_{G_F}^{\infty}(\varepsilon_0)) \left(F_{G_F}^{\infty}(\varepsilon_0) - F_{G_F}^{\infty} \left(\frac{\Theta_B}{\rho} \right) \right) \\
&\approx F_{G_B}^{\infty}(\varepsilon_0) - F_{G_B}^{\infty}(\varepsilon_1) + F_{G_F}^{\infty}(\varepsilon_0) \\
&\quad - F_{G_F}^{\infty} \left(\frac{\Theta_B}{\rho} \right) - A_1 \sum_{i=0}^{m-1} \frac{(\lambda_F)^i \Phi_2^{\infty}}{i!} \\
&= \frac{\lambda_B^m (\varepsilon_0^m - \varepsilon_1^m)}{m!} + \frac{\lambda_F^m}{m!} \left(\varepsilon_0^m - \frac{\Theta_B^m}{\rho^m} \right) \\
&\quad - A_1 \sum_{i=0}^{m-1} \frac{\lambda_F^i \Phi_2^{\infty}}{i!}
\end{aligned} \tag{59}$$

where $\Phi_2^{\infty} = \frac{\varepsilon_0^{i+m} - \varepsilon_1^{i+m}}{i+m}$.

REFERENCES

- [1] Q. Wu, J. Xu, Y. Zeng, D. W. K. Ng, N. Al-Dhahir, R. Schober, and A. L. Swindlehurst, "A comprehensive overview on 5G-and-beyond networks With UAVs: From Communications to sensing and intelligence," IEEE J. Sel. Areas Commun., 39 (10) (2021) 2912-2945.
- [2] Y. Liu, Z. Qin, Y. Cai, Y. Gao, G. Y. Li, and A. Nallanathan, "UAV communications based on non-orthogonal multiple access," IEEE Wireless Commun., 26 (1) (2019) 52-57.
- [3] Z. Ding, Y. Liu, J. Choi, Q. Sun, M. Elkashlan, C.-L. I, and H. V. Poor, "Application of non-orthogonal multiple access in LTE and 5G networks," IEEE Commun. Mag., 55 (2) (2017) 185-191.
- [4] T. Hou, Y. Liu, Z. Song, X. Sun, and Y. Chen, "Multiple antenna aided NOMA in UAV networks: A stochastic geometry approach," IEEE Trans. Commun., 67 (2) (2019) 1031-1044.
- [5] T. Hou, Y. Liu, Z. Song, X. Sun, and Y. Chen, "UAV-to-everything (U2X) networks relying on NOMA: A stochastic geometry model," IEEE Trans. Veh. Technol., 69 (7) (2020) 7558-7568.

$$\begin{aligned}
T_{2a}^b &= \Pr \left\{ G_F < \frac{\Theta_B G_B}{\rho G_B + 1}, \varepsilon_1 < G_B < \varepsilon_6 \right\} + \Pr \left\{ G_F < \frac{\varepsilon_4 G_B}{G_B - \varepsilon_3}, G_B > \varepsilon_6 \right\} \\
&= \int_{\varepsilon_1}^{\varepsilon_6} f_{G_B}(y) F_{G_F} \left(\frac{\Theta_B y}{\rho y + 1} \right) dy + \int_{\varepsilon_6}^{\infty} f_{G_B}(y) F_{G_F} \left(\frac{\varepsilon_4 y}{y - \varepsilon_3} \right) dy \\
&= \int_{\varepsilon_1}^{\infty} f_{G_B}(y) dy - \frac{\lambda_B^m}{\Gamma(m)} \sum_{i=0}^{m-1} \frac{(\lambda_F \Theta_B)^i}{\rho^i i!} \int_{\varepsilon_1}^{\varepsilon_6} y^{m-1} e^{-\lambda_B y - \frac{\lambda_F \Theta_B y}{y + \frac{1}{\rho}}} \frac{y^{m+i-1}}{\left(y + \frac{1}{\rho}\right)^i} dy \\
&\quad - \frac{\lambda_B^m}{\Gamma(m)} \sum_{i=0}^{m-1} \frac{(\lambda_F \varepsilon_4)^i}{i!} \int_{\varepsilon_6}^{\infty} e^{-\lambda_B y - \frac{\lambda_F \varepsilon_4 y}{y - \varepsilon_3}} \frac{y^{m+i-1}}{(y - \varepsilon_3)^i} dy \\
&= \bar{F}_{G_B}(\varepsilon_1) - A_1 g_1 \left(-\frac{1}{\rho}, \frac{\Theta_B}{\rho}, \varepsilon_1, \varepsilon_6 \right) - A_1 g_2(\varepsilon_3, \varepsilon_4, \varepsilon_6)
\end{aligned} \tag{53}$$

$$\begin{aligned}
T_3 &= \Pr \left\{ G_B > \varepsilon_1, \frac{\Theta_B G_B}{\rho G_B + 1} < G_F < G_B, G_F < \varepsilon_0 \right\} \\
&= \Pr \left\{ \frac{\Theta_B G_B}{\rho G_B + 1} < G_F < G_B, \varepsilon_1 < G_B < \varepsilon_0 \right\} + \Pr \left\{ \frac{\Theta_B G_B}{\rho G_B + 1} < G_F < \varepsilon_0, G_B > \varepsilon_0 \right\} \\
&= F_{G_F}(\varepsilon_0) \int_{\varepsilon_0}^{\infty} f_{G_B}(y) dy + \int_{\varepsilon_1}^{\varepsilon_0} f_{G_B}(y) F_{G_F}(y) dy - \int_{\varepsilon_1}^{\infty} f_{G_B}(y) F_{G_F} \left(\frac{\Theta_B y}{\rho y + 1} \right) dy \\
&= F_{G_F}(\varepsilon_0) \bar{F}_{G_B}(\varepsilon_0) + \int_{\varepsilon_1}^{\varepsilon_0} f_{G_B}(y) F_{G_F}(y) dy - \left(1 - F_{G_B}(\varepsilon_1) - \frac{\lambda_B^m}{\Gamma(m)} \sum_{i=0}^{m-1} \frac{(\lambda_F)^i \Phi_2}{i!} \right) \\
&= A_1 \Phi_5 - \bar{F}_{G_F}(\varepsilon_0) \bar{F}_{G_B}(\varepsilon_0) - A_1 \sum_{i=0}^{m-1} \frac{(\lambda_F)^i \Phi_2}{i!}
\end{aligned} \tag{55}$$

-
- [6] T. Hou, Y. Liu, Z. Song, X. Sun, and Y. Chen, "Exploiting NOMA for UAV communications in large-scale cellular networks," *IEEE Trans. Commun.*, 67 (10) (2019) 6897-6911.
- [7] T. Hou, Y. Liu, Z. Song, X. Sun, and Y. Chen, "NOMA-enhanced terrestrial and aerial IoT networks with partial CSI," *IEEE Internet Things J.*, 7 (4) (2020) 3254-3266.
- [8] W. U. Khan, N. Imtiaz, and I. Ullah, "Joint optimization of NOMA-enabled backscatter communications for beyond 5G IoT networks," *Internet Technol. Lett.*, 4 (2) (2021) e265.
- [9] N. Zhao, X. Pang, Z. Li, Y. Chen, F. Li, Z. Ding, and M.-S. Alouini, "Joint trajectory and precoding optimization for UAV-assisted NOMA networks," *IEEE Trans. Commun.*, 67 (5) (2019) 3723-3735.
- [10] D. Zhai, H. Li, X. Tang, R. Zhang, Z. Ding, and F. R. Yu, "Height optimization and resource allocation for NOMA enhanced UAV-aided relay networks," *IEEE Trans. Commun.*, 69 (2) (2021) 962-975.
- [11] H. Zhang, J. Zhang, and K. Long, "Energy efficiency optimization for NOMA UAV network with imperfect CSI," *IEEE J. Sel. Areas Commun.*, 38 (12) (2020) 2798-2809.
- [12] W. Wang, N. Zhao, L. Chen, X. Liu, Y. Chen, and D. Niyato, "UAV-assisted time-efficient data collection via uplink NOMA," *IEEE Trans. Commun.*, 69 (11) (2021) 7851-7863.
- [13] M. Liu, G. Gui, N. Zhao, J. Sun, H. Gacanin, and H. Sari, "UAV-aided air-to-ground cooperative nonorthogonal multiple access," *IEEE Internet Things J.*, 7 (4) (2020) 2704-2715.
- [14] M. Shirvanimoghaddam, M. Dohler, and S. J. Johnson, "Massive non-orthogonal multiple access for cellular IoT: Potentials and limitations," *IEEE Commun. Mag.*, 55 (9) (2017) 55-61.
- [15] D. Park, H. Seo, H. Kwon, and B. G. Lee, "Wireless packet scheduling based on the cumulative distribution function of user transmission rates," *IEEE Trans. Commun.*, 53 (11) (2005) 1919-1929.
- [16] Z. Ding, R. Schober, and H. V. Poor, "A new QoS-guarantee strategy for NOMA assisted semi-grant-free transmission," *IEEE Trans. Commun.*, 69 (11) (2021) 7489-7503.
- [17] Y. Sun, Z. Ding, and X. Dai, "A new design of hybrid SIC for improving transmission robustness in uplink NOMA," *IEEE Trans. Veh. Technol.*, 70 (5) (2021) 5083-5087.
- [18] Z. Yang, P. Xu, J. Ahmed Hussein, Y. Wu, Z. Ding, and P. Fan, "Adaptive power allocation for uplink non-orthogonal multiple access with semi-grant-free transmission," *IEEE Wireless Commun. Lett.*, 9 (10) (2020) 1725-1729.
- [19] H. Lu, X. Xie, Z. Shi, H. Lei, H. Yang, and J. Cai, "Advanced NOMA assisted semi-grant-free transmission schemes for randomly distributed users," *IEEE Trans. Wireless Commun.*, 22 (7) (2023) 4638-4653.
- [20] C. Zhang, Y. Liu, and Z. Ding, "Semi-grant-free NOMA: A stochastic geometry model," *IEEE Trans. Wireless Commun.*, 21 (2) (2022) 1197-1213.
- [21] C. Zhang, Y. Liu, W. Yi, Z. Qin, and Z. Ding, "Semi-grant-free NOMA: Ergodic rates analysis with random deployed users," *IEEE Wireless Commun. Lett.*, 10 (4) (2021) 692-695.
- [22] H. Lei, F. Yang, H. Liu, I. Shafique Ansari, K. J. Kim, and T. A. Tsiftsis, "On secure NOMA-aided semi-grant-free systems," *IEEE Trans. Wireless Commun.*, doi: 10.1109/twc.2023.3275946, (2023) 1-17.
- [23] J. Chen, L. Guo, J. Jia, J. Shang, and X. Wang, "Resource allocation for IRS assisted SGF NOMA transmission: A MADRL approach," *IEEE J. Sel. Areas Commun.*, 40 (4) (2022) 1302-1316.
- [24] X. Yue, Z. Qin, Y. Liu, S. Kang, and Y. Chen, "A unified framework for non-orthogonal multiple access," *IEEE Trans. Commun.*, 66 (11) (2018) 5346-5359.
- [25] X. Yue, Y. Liu, Y. Yao, X. Li, R. Liu, and A. Nallanathan, "Secure communications in a unified non-orthogonal multiple access framework," *IEEE Trans. Wireless Commun.*, 19 (3) (2020) 2163-2178.
- [26] M. Vaezi, R. Schober, Z. Ding, and H. V. Poor, "Non-orthogonal multiple access: Common myths and critical questions," *IEEE Wireless Commun.*, 26 (5) (2019) 174-180.
- [27] Y. Zhou, P. L. Yeoh, H. Chen, Y. Li, R. Schober, L. Zhuo, and B. Vucetic, "Improving physical layer security via a UAV friendly jammer for unknown eavesdropper location," *IEEE Trans. Veh. Technol.*, 67 (11) (2018) 11280-11284.
- [28] A. Al-Hourani, S. Kandeepan, and S. Lardner, "Optimal LAP altitude for maximum coverage," *IEEE Wireless Commun. Lett.*, 3 (6) (2014) 569-572.
- [29] M. Azari, F. Rosas, K.-C. Chen, and S. Pollin, "Ultra reliable UAV communication using altitude and cooperation diversity," *IEEE Trans. Commun.*, 66 (1) (2018) 330-344.
-

- [30] I. S. Gradshteyn and I. M. Ryzhik, Table of Integrals, Series and Products, 7th. San Diego, CA: Academic Press, 2007.
- [31] M. Abramowitz and I. A. Stegun, Handbook of Mathematical Functions with Formulas, Graphs, and Mathematical Tables, 9th. New York, NY, USA: Dover Press, 1972.